



UNIVERSITY OF LEEDS

This is a repository copy of *A Link Between the Tribology and Corrosive Degradation of Metal-on-Metal THRs*.

White Rose Research Online URL for this paper:

<https://eprints.whiterose.ac.uk/111363/>

Version: Accepted Version

Article:

Beadling, AR orcid.org/0000-0001-5501-0140, Bryant, MG orcid.org/0000-0003-4442-5169, Dowson, D orcid.org/0000-0001-5043-5684 et al. (1 more author) (2017) *A Link Between the Tribology and Corrosive Degradation of Metal-on-Metal THRs*. *Tribology International*, 113. pp. 354-361. ISSN 0301-679X

<https://doi.org/10.1016/j.triboint.2017.01.028>

© 2017 Elsevier Ltd. This manuscript version is made available under the CC-BY-NC-ND 4.0 license <http://creativecommons.org/licenses/by-nc-nd/4.0/>

Reuse

Items deposited in White Rose Research Online are protected by copyright, with all rights reserved unless indicated otherwise. They may be downloaded and/or printed for private study, or other acts as permitted by national copyright laws. The publisher or other rights holders may allow further reproduction and re-use of the full text version. This is indicated by the licence information on the White Rose Research Online record for the item.

Takedown

If you consider content in White Rose Research Online to be in breach of UK law, please notify us by emailing eprints@whiterose.ac.uk including the URL of the record and the reason for the withdrawal request.

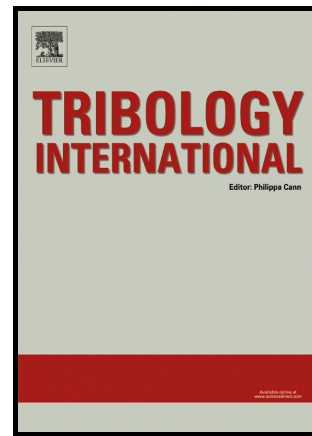


eprints@whiterose.ac.uk
<https://eprints.whiterose.ac.uk/>

Author's Accepted Manuscript

A Link Between the Tribology and Corrosive Degradation of Metal-on-Metal THRs

A.R. Beadling, M.G. Bryant, D. Dowson, A. Neville



www.elsevier.com/locate/jtri

PII: S0301-679X(17)30037-3
DOI: <http://dx.doi.org/10.1016/j.triboint.2017.01.028>
Reference: JTRI4568

To appear in: *Tribology International*

Received date: 13 July 2016
Revised date: 19 January 2017
Accepted date: 23 January 2017

Cite this article as: A.R. Beadling, M.G. Bryant, D. Dowson and A. Neville, A Link Between the Tribology and Corrosive Degradation of Metal-on-Metal THRs, *Tribology International*, <http://dx.doi.org/10.1016/j.triboint.2017.01.028>

This is a PDF file of an unedited manuscript that has been accepted for publication. As a service to our customers we are providing this early version of the manuscript. The manuscript will undergo copyediting, typesetting, and review of the resulting galley proof before it is published in its final citable form. Please note that during the production process errors may be discovered which could affect the content, and all legal disclaimers that apply to the journal pertain

A Link Between the Tribology and Corrosive Degradation of Metal-on-Metal THR[☆]

A. R. Beadling^{a,*}, M. G. Bryant^a, D. Dowson^a, A. Neville^a

^a*Institute of Functional Surfaces, University of Leeds, UK*

Abstract

The degradation of Metal-on-Metal (MoM) Total Hip Replacements (THR) is a complex mix of tribological, corrosive phenomena and their synergistic processes. Previous links between the corrosion of these devices and their sliding conditions over a cycle have been observed in simulator studies instrumented with a three-electrode electrochemical cell. This study further quantifies that link; demonstrating clear repeating periodicity in the anodic current transients of a 28 mm diameter MoM bearing under a standard ISO-14242 walking profile. A simplified 2D model and an expression of the Hamrock-Dowson equation was utilised to estimate the Theoretical Minimum Film Thickness (h_{min}) over a cycle, which was shown to match closely to the measured anodic current in both shape and magnitude.

Keywords: Metal-on-Metal, Biotribocorrosion, Total Hip Replacement

1. Introduction

After discovering higher than acceptable revision rates for Metal-on-Metal (MoM) bearings in Total Hip Replacement (THR) there has been a rapid decline in their use over the past decade [2, 3]. Despite this 1,096 MoM primary hip replacement operations were performed in the UK in 2014 [4]. Whilst this only accounts for 1.16 % of the total operations performed that year, MoM devices are still being used and thousands are still implanted in patients world wide. Thus there has been a large focus in the literature on explaining their higher than acceptable revision rates. Several simulator studies have examined MoM devices in adverse loading scenar-

ios and demonstrated increased wear rates. Bowsher *et al.* [5] demonstrated a seven-fold increase in volumetric wear for 40 mm MoM bearings due to a fast-jogging profile. This was also coupled with a twenty-fold increase in wear particle surface area; likely resulting in increased release of metal ions. Of particular note are microseparation and malpositioning of these devices, either due to sub-optimal placement during surgery or component migration. Angadji *et al.* [6] demonstrated a three and seven-fold increase in steady-state volumetric wear rate for 40 mm MoM bearings by increasing the angle of acetabular inclination from 35° to 50 and 60° respectively. Williams *et al.* [7] and Al-Hajjar *et al.* [8] both demonstrated three to five fold increases in steady-state volumetric wear for 28 mm diameter MoM bearings with high acetabular inclination or by applying microseparation.

[☆]The data associated with this paper are openly available from the University of Leeds data repository. <http://doi.org/10.5518/88> [1].

*Corresponding author

Email address: a.r.beadling@leeds.ac.uk (A. R. Beadling)

Whilst significant, these wear rates are still fractions of those noted for typical Metal-on-Polymer designs. During pre-clinical testing of MoM devices the low wear rate and wear particle size distributions were used to demonstrate their suitability for younger and more active patients [9, 10, 11, 12]. That promise did not translate into clinical success and younger patients demonstrated some of the worst MoM failure rates [2, 3, 13]. Gravimetric assessment of metallic devices after continuous 1 Hz simulator testing may not fully capture the degradation mechanisms at the interface or be indicative of how well these devices perform *in-vivo*.

This group has attempted to quantify the corrosive degradation of MoM bearings by instrumenting various hip simulators with a three-electrode electrochemical cell. This facilitates *in-situ* monitoring of corrosive processes from the device and allows the estimation of the contribution of corrosion to total material loss. Third-body wear debris and higher loading conditions were found to greatly increase the direct release of metallic ions into the lubricant [14, 15]. The effect of corrosion has also been observed to change over the course of long-term simulator tests with marked shifts in Open Circuit Potential and corrosion current during running-in of the device [16]. Adverse loading scenarios have also been observed to increase the percentage contribution of corrosion to total degradation [17]. This has all combined to demonstrate the importance of *in-situ* corrosion monitoring as a tool to aid assessment of implant performance [18].

A comprehensive model which links the corrosive degradation of a metal sliding contact to total wear has therefore long been a goal. Hesketh *et al.* [19, 20] made an initial attempt to correlate repeating patterns noted in anodic currents measured from Metal-on-Metal bear-

ings with a so called ‘severity factor.’

$$I \propto \frac{W\omega}{h_{min}} \quad (1)$$

where I is the current generated by sliding (amps), W is the axial load (N), ω is the angular velocity ($\text{rad}\cdot\text{s}^{-1}$) and h_{min} is the theoretical minimum film thickness (nm). As conditions become more severe at the interface, i.e. load increases or the lubricating film thickness reduces, this should cause an increase in depassivation of the surface and correspond to an increase in the measured anodic current transient. The ‘severity factor’ demonstrated a similar shaped profile to anodic current transients. The peaks did not appear to align however, and the onset of current was often in advance of high severity portions of the cycle. This noted phase difference was not well understood as current should align with or follow surface damage. This study aimed to further understand this observed link between corrosive degradation and the tribological conditions over the course of a cycle.

2. Material and methods

2.1. Material

A 28 mm diameter Metal-on-Metal device was placed in a Full-ISO Electromechanical Hip Simulator (ProSim, UK). The bearing comprised of a Cobalt Chromium Molybdenum alloy (*CoCrMo*) Femoral Head and Acetabular Liner. Polyether ether ketone (PEEK) fixtures were used to electrochemically isolate the components from the simulator. The liner was held in place by a Titanium alloy (*Ti6Al4V*) Acetabular Shell which was cemented into the cup fixture using laboratory grade Poly(methyl methacrylate) (PMMA) bone cement. The Femoral Head was held in place using

a 316L Stainless Steel spigot. Care was taken to seal the modular taper connections with silicone sealant to prevent the ingress of lubricant into the modular taper. Thus the taper interface did not form part of the electrochemical cell and any electrochemical measurements only concerned the bearing surface. The lubricant used was Foetal Bovine Serum (FBS) diluted to 17 gL^{-1} total protein content with Phosphate Buffered Saline (PBS) to facilitate electrochemical measurement. The protein content of the lubricant was selected as per the qualification previously set by Hesketh *et al.* [16, 20]. Sodium Azide (NaN_3 , 0.03 % (w/v)) was also added in order to retard bacterial growth.

2.2. Methods

The simulator was instrumented with a three-electrode electrochemical cell to facilitate *in-situ* measurements of corrosive degradation. A working electrode (WE) connection was taken from both the Acetabular Shell and the 316L Stainless Steel spigot. An illustration of the test cell can be seen in Figure 1. The working electrode therefore comprised of all component surfaces present in the cell which were exposed to the lubricant. A combination Silver/Silver Chloride (Ag/AgCl) reference electrode (RE) and Platinum (Pt) counter electrode (CE) completed the cell. All measurements were performed using a PGSTAT101 Potentiostat (Metrohm Autolab, Netherlands).

To begin the 'bedding-in' process the bearing was articulated under a standard ISO 14242-1 [21] loading profile, shown in Figure 2, for 333,000 cycles at 1 Hz. This consisted of a twin-peak loading curve with 3,000 N peak loads at 'heel-strike' and 'toe-off' and a 300 N swing phase load. The rotational axes were $+25^\circ/-18^\circ$ Flexion/Extension, $+7^\circ/-4^\circ$ Adduction/Abduction and

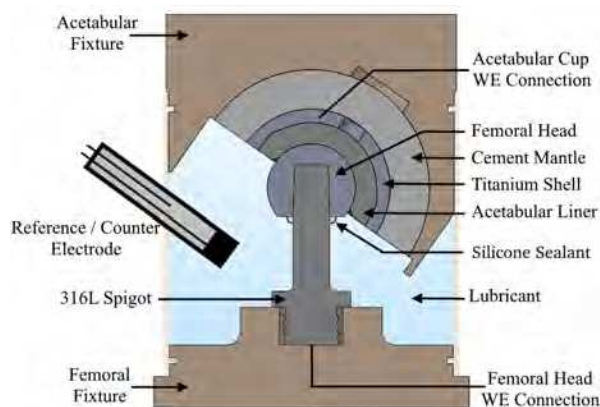


Figure 1: Schematic Illustration of the Hip Simulator test cell.

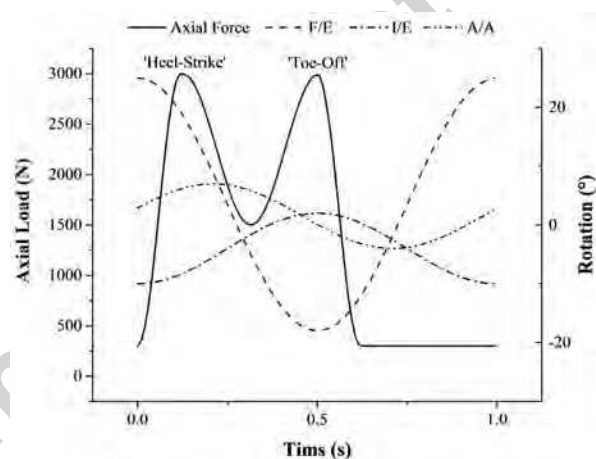


Figure 2: Standard ISO 14242-1 Walking Profile [21].

$+2^\circ/-10^\circ$ Internal/External Rotation.

The hypothesis of this study was that the phase difference between current and 'severity factor' was a lag following from the previous cycle, rather than advance peaks of current. In order to determine if the phase difference was purely a time delay in the electrochemical cell or a function of the cycle tribology the bearing was run at different cycle frequencies; ranging from 0.4 to 1.4 Hz. The Open Circuit Potential (OCP) was continuously monitored for 1,800 seconds at 1 Hz during sliding.

Finally an anodic over potential of +50 mV vs. OCP

was applied to the working electrode during sliding.

145 The resultant anodic current transient was sampled at 100 Hz. The resultant current was governed by the Butler-Volmer equation (Equation 2) and enabled monitoring of the depassivation/repassivation kinetics during a cycle.

$$150 \quad I = I_{corr} \left\{ \exp \left(\frac{\alpha_a n F \eta}{RT} \right) - \exp \left(- \frac{\alpha_c n F \eta}{RT} \right) \right\} \quad (2)$$

where I is the current as a result of applied potential (amps), I_{corr} is the corrosion current at OCP (amps), α_a and α_c are the anodic and cathodic charge transfer coefficients, n is the number of electrons in the half-cell reaction, F is Faraday's Constant (96,490 C/mol), η is the applied overpotential (V), R is the Ideal Gas Constant and T is the temperature (Kelvin). In order to synchronise the measured current with the point in the cycle a direct analogue voltage signal for Axial Load was taken from the simulator load cell and sampled by the potentiostat at 100 Hz along with the current.

A series of three daily living scenarios were also examined under the same testing method. They consisted of a 'Physiological Gait' profile at 1 Hz, a 'Stair Climb' profile at 0.666 Hz, and a combined 'Chair Down - Up' profile at 0.5 Hz. These profiles were derived from data provided by Fabry *et al.* [22] which was based on the work of Bergmann *et al.* [23, 24].

2.3. Hamrock-Dowson Model

170 A simplified 2D model, shown in Figure 4, was utilised in an attempt to correlate the tribology at a given point in a cycle with the electrochemical degradation. An expression of the Hamrock-Dowson equation (Equation 3) [25] was used to estimate the minimum film thickness over three cycles.

$$175 \quad h_{min} = 2.8R' \left(\frac{\eta u}{E'R'} \right)^{0.65} \left(\frac{W}{E'R'^2} \right)^{-0.21} \quad (3)$$

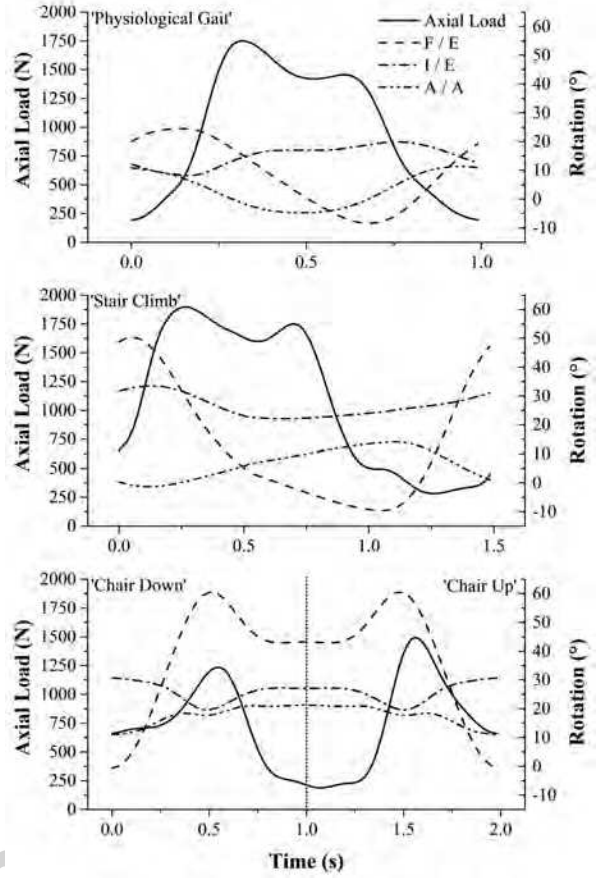


Figure 3: Daily Living profiles derived from data provided by Fabry *et al.* [22].

where R' is the Equivalent Radius (m), η is the Lubricant Viscosity (0.005 Pa.s), u is the Entraining Velocity (ms^{-1}) and E' is the Equivalent Elastic Modulus (Pa). R' and E' are derived from Equations 4 and 5 respectively:

$$180 \quad R' = \frac{r_1 r_2}{r_2 - r_1} \quad (4)$$

$$E' = 2 \left(\frac{1 - \nu_1^2}{E_1} + \frac{1 - \nu_2^2}{E_2} \right) \quad (5)$$

where r_1 , E_1 and ν_1 are the radius (m), Elastic Modulus (Pa) and Poisson's Ratio for the Femoral Head and r_2 , E_2 and ν_2 are the radius (m), Elastic Modulus (Pa) and Poisson's Ratio for the Acetabular Cup.

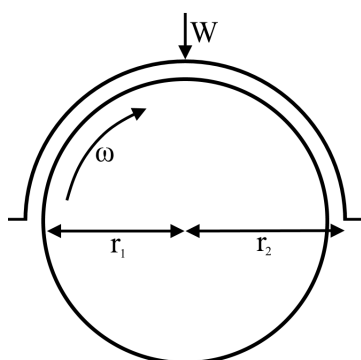


Figure 4: Schematic of the simplified 2D model for a Femoral Head articulating within an Acetabular Cup.

Standard values of Young's Modulus and Poisson's Ratio for *CoCrMo* alloy were used (230 MPa, 0.3) and a diametrical clearance of 100 μm was taken. In order to calculate the lubricant entrainment velocity (u) at each point in the cycle the change in position for each rotational axis was used to calculate an angular velocity (ω). This was then converted to a sliding speed for each axis for the 28 mm diameter bearing and combined to give a resultant vector.

The minimum film thickness was then inverted ($1/h_{min}$) in order to give peaks at points in the cycle when the film was thinnest. This would correspond to more asperity-asperity contact during sliding and thus more depassivation of the surface; represented by peaks in current. The data associated with this paper are openly available from the University of Leeds data repository. <http://doi.org/10.5518/88> [1].

3. Results

3.1. OCP

Once sliding was initiated a cathodic shift in OCP was noted at all frequencies. At the lower cycle frequencies however (< 1.0 Hz) larger and more sustained

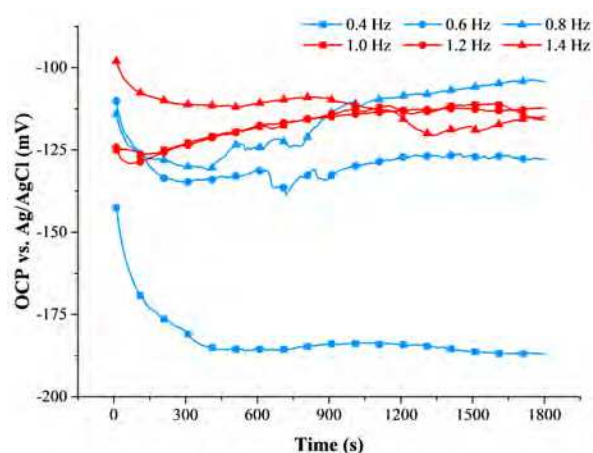


Figure 5: Open Circuit Potential for a bed-in 28 mm MoM bearing articulating under an ISO 14242-1 profile at cycle frequencies ranging from 0.4 to 1.4 Hz.

cathodic shifts were observed. At 0.4 Hz for example the OCP shifted cathodically to approximately -185 mV and remained stable there during sliding. At 0.6 and 0.8 Hz there were also larger cathodic shifts but the OCP gradually shifted more noble to similar values noted for the standard 1.0 Hz (≈ -100 to -130 mV). At 1.4 Hz this relationship appeared to change with a slight cathodic shift upon sliding and then continued to shift cathodically over the remainder of the experiment. The larger and more sustained cathodic shifts appeared to result in larger anodic current transients, shown in Figure 6.

3.2. Anodic Polarisation

At all but one cycle frequency a twin peak profile was noted with a primary peak at 'toe-off' and a typically larger secondary peak at the initiation of 'heel-strike' of the next cycle. At 0.4 Hz a third peak was observed inbetween the primary and secondary peaks at the commencement of the swing phase portion of the cycle. The position of the peaks in anodic current remained fairly consistent between the other frequencies and occurred

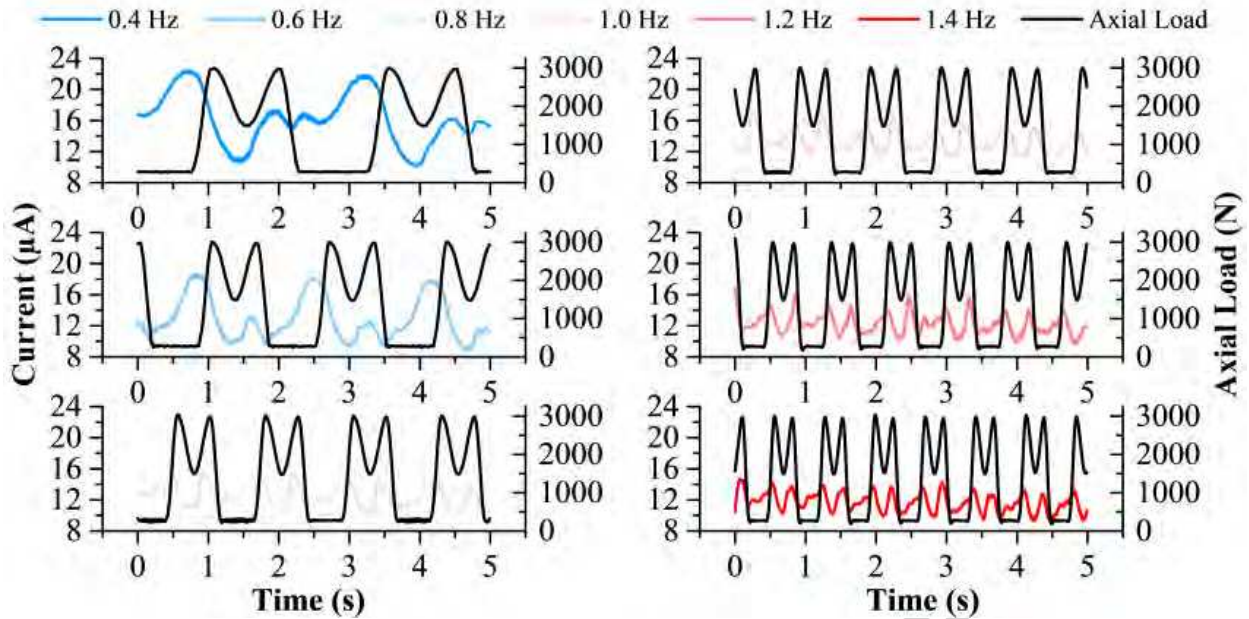


Figure 6: Anodic Current Transient (+50 mV vs. OCP) and Axial Load for a 28 mm MoM bearing under an ISO 14242-1 profile at cycle frequencies ranging from 0.4 to 1.4 Hz.

at similar points in the cycle. A trend of decreasing anodic current magnitude with increasing cycle frequency was also noted. The time delay between ‘heel-strike’ and ‘toe-off’ peaks in load and the following primary and secondary peaks in current was recorded for all frequencies and is shown in Figure 7. The delay between the peaks decreased with increasing cycle frequency.

Figure 8 shows the peak anodic currents and initial OCP cathodic shift for each frequency. These values are plotted against the maximum entrainment velocity (u) over a cycle, determined by Equation 3. As described above, greater initial cathodic shifts in OCP were observed when reducing the cycle frequency from 1.0 Hz. This was coupled with an increase in the peak anodic current noted during polarisation after 1,800 seconds. Increasing the frequency from 1.0 Hz also resulted in larger initial cathodic shifts at 1.2 and 1.4 Hz, but the peak anodic current continued to fall possibly due to

changes in the lubrication regime.

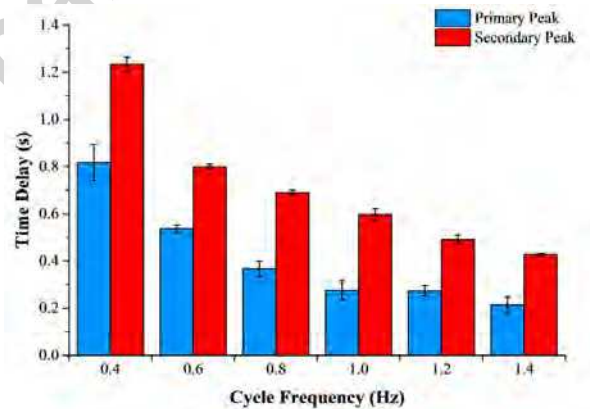


Figure 7: Time delay between peaks in Axial Load and Anodic Current Transient for different cycle frequencies.

3.3. Hamrock-Dowson Model

Figure 9 shows the axial load and calculated resultant entrainment velocity over three cycles for each cycle frequency. An assumption of the Hamrock-Dowson equation is that the system is in steady-state and neglects

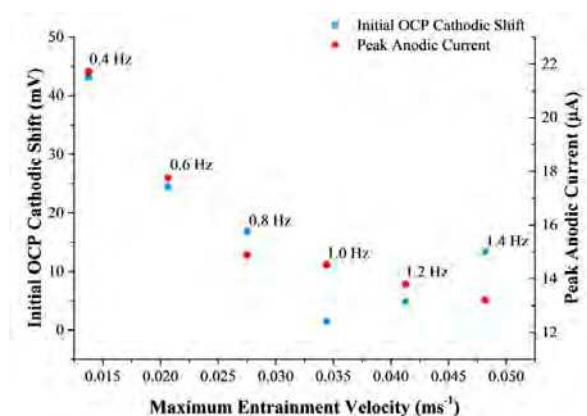


Figure 8: Initial OCP Cathodic Shift and Peak Anodic Current for a 28 mm MoM bearing under an ISO 14242-1 profile at cycle frequencies ranging from 0.4 to 1.4 Hz.

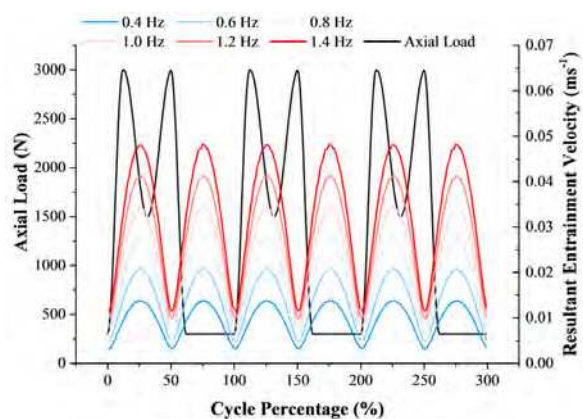


Figure 9: Axial Load and Resultant Entrainment Velocity at the contact for a 28 mm MoM bearing articulating under an ISO 14242-1 profile at cycle frequencies ranging from 0.4 to 1.4 Hz.

phenomena such as squeeze film. The lubricant is also
 255 assumed to have a constant viscosity and entrainment
 occurs at a 1:1 ratio with angular velocity. Thus the
 shape and locations of peaks in entrainment velocity did
 not vary but the magnitude of those peaks did change. 280
 The maximum entrainment velocity at each frequency
 varied to a much larger degree than the minimum, in-
 260 creasing from approximately 0.014 to 0.048 ms⁻¹. The
 points of minimum entrainment occurred at approxi-
 mately 50 and 100 % through each cycle, i.e. at ‘toe-off’
 and the initiation of ‘heel-strike’ for the next cycle. This 285
 corresponded to the peaks in anodic current for each fre-
 265 quency noted in Figure 6.

The inverted minimum film thickness appeared to
 give a much better correlation between the anodic cur-
 rent and the tribological conditions at a given point in 290
 the cycle than the ‘severity factor’ previously proposed
 by Hesketh *et al.* [19, 20]. Figure 10 shows for each
 270 cycle frequency the peaks in anodic current aligned rea-
 sonably well with points of minimum film thickness.

The magnitude of current also appeared to scale with 295
 275 the magnitude of inverted film thickness between the cy-

cle frequencies. Moving from 0.4 to 1.4 Hz the peak an-
 odic current fell from approximately 22 to 13 µA. The
 maximum inverted film thickness also fell from approx-
 imately 0.15 to 0.06 nm⁻¹. When viewed on the same
 scale, as in Figure 10, there appeared to be a good corre-
 lation between the overall tribological severity at a given
 frequency and the resultant anodic current.

3.4. Daily Living Cycles

Figures 11, 12 and 13 show the anodic current tran-
 sients and inverted film thickness as a function of cy-
 cle percentage for ‘physiological gait,’ ‘stair climb’ and
 ‘chair down - up’ profiles respectively.

Under ‘physiological gait’ the shape of the anodic
 current transient was different to those noted for ISO
 14242-1 profiles. The transient appeared to only consist
 of a single peak of approximately 30 µA which occurred
 at the initiation of ‘heel-strike.’ This peak in current
 aligned with a peak in the inverted film thickness, al-
 though the model appeared to break down further in
 the cycle. A second peak in inverted film thickness was
 noted approximately at ‘toe-off’ but was not coupled

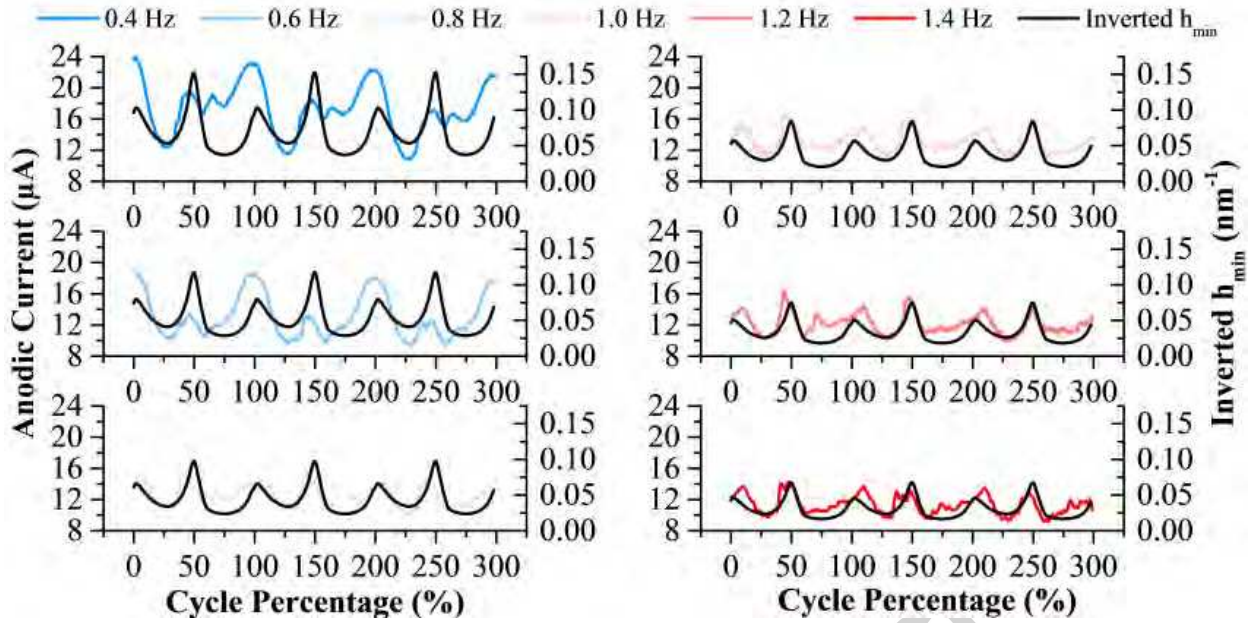


Figure 10: Anodic Current Transient (+50 mV vs. OCP) and Inverted Theoretical Minimum Film Thickness for a 28 mm MoM bearing under an ISO 14242-1 profile at cycle frequencies ranging from 0.4 to 1.4 Hz.

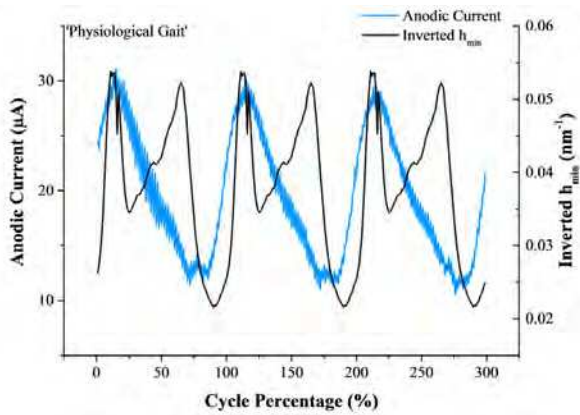


Figure 11: Anodic Current Transient (+50 mV vs. OCP) and Inverted Theoretical Minimum Film Thickness for a 28 mm MoM bearing under a 'Physiological Gait' cycle derived from data provided by Fabry *et al.* [22].

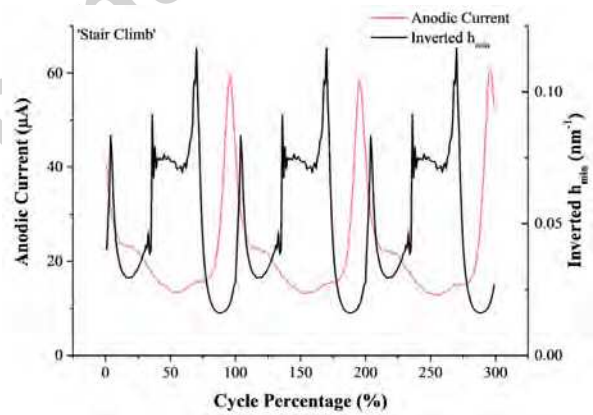


Figure 12: Anodic Current Transient (+50 mV vs. OCP) and Inverted Theoretical Minimum Film Thickness for a 28 mm MoM bearing under a 'Stair Climb' cycle derived from data provided by Fabry *et al.* [22].

with a peak in current, which continued to fall until the next 'heel-strike.' There was a slight change to the current curve around this point but was not a clearly well defined peak. Both of the inverted film thickness peaks occurred approximately at points of maximum and min-

imum Flexion / Extension; at where the entrainment velocity was at a minimum. The simplicity of the model may have underestimated the film thickness at the 'toe-off' point of the more complex physiological profile.

Under the 'stair climb' profile the current transient

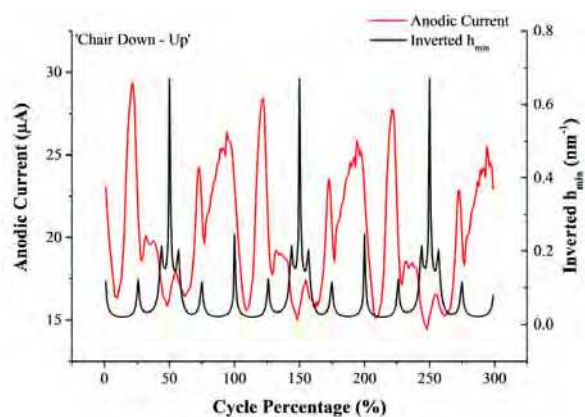


Figure 13: Anodic Current Transient (+50 mV vs. OCP) and Inverted Theoretical Minimum Film Thickness for a 28 mm MoM bearing under a 'Chair Down - Up' cycle derived from data provided by Fabry *et al.* [22].

took on a completely new shape, not seen previously. A large primary peak initiated just after the 'toe-off' point approximately 75 % through each cycle. The magnitude of this peak was also double that of 'physiological gait' at approximately 59 μA . A much smaller secondary peak was observed soon after at approximately 20 % through each cycle. Again the simplified 2D model for inverted film thickness did not appear to align with the current transient and showed completely different shapes and peaks that occurred at different points through each cycle.

The anodic current transient for the 'chair down - up' profile demonstrated multiple peaks throughout each cycle ranging from 17.5 μA to 28 - 29 μA . Some of the peaks were also fairly broad and occurred over as much as 50 % of each cycle which would translate to high corrosive material loss. Whilst again there did not appear to be a good alignment between the current and the inverted film thickness, the simplified model did appear to pick up on the complex nature of the profile; resulting in several points of minimum film thickness.

4. Discussion

The present study has shown that there is a close link between the electrochemical degradation and the tribological conditions at the bearing surface of a Metal-on-Metal device. The simplified 2D model used to estimate the theoretical minimum film thickness showed close agreement to the anodic current transients captured for the 28 mm diameter bearing articulated under the ISO walking profile. This appeared to confirm that at these points in each cycle more asperity-asperity contact occurred as a result of a thinner lubricating film and resulted in more severe depassivation of the protective oxide layer and thus greater corrosive degradation at the sliding interface. At all but the slowest frequency (0.4 Hz) a clear repeating two-peak shape was noted both in the inverted film thickness and anodic current. The anodic current transients shown in Figure 6 closely matched typical shapes seen in previous studies on a pneumatic simulator for 28 mm MoM bearings [17]. The position of both primary and secondary peaks aligned reasonably well at similar points in the cycle. Also the magnitude of the peaks scaled similarly between the frequencies under ISO walking after bedding-in.

The reduction in time delay observed between peaks in load and the primary and secondary peaks in current, shown in Figure 7, further suggests a response to the tribology at that point in the cycle. Had the phase difference been purely a time delay inherent in the electrochemical cell, the current peaks would have been expected to occur a fixed time after a peak in load for all frequencies. This did not appear to be the case and in fact the time delay reduced at a similar ratio to the increase in cycle frequency. This further suggested that

the peaks were occurring at the same point in the cycle, rather than being delayed after the loading peak. They were therefore not thought to be simply out of phase with the load, but a response to some other tribological factor at that point in the cycle. The ‘severity factor’ first proposed by Hesketh *et al.* was a first attempt to characterise this and link it to the corrosive degradation. The ‘severity factor’ appeared to be similarly inadequate as simply syncing to the loading curve. Both axial load and angular velocity, components of the severity factory, are functions of the minimum film thickness. Current peaks also appeared to occur at points of minimum entrainment, rather than maximum load or ‘severity.’ An inverted film thickness parameter therefore appears better suited to describing the tribological conditions at the interface for tribocorrosion.

Determining film thickness is not a trivial task; especially for the 28 mm bearing used in the present study for example which operates typically in a mixed lubrication regime. Whilst the simplified 2D model may have shown good agreement across the different ISO profile frequencies, when applied to the daily living profiles the model broke down. Under ‘physiological gait’ a secondary peak in inverted film thickness was not found in the anodic current transient. The profile shape for ‘stair climb’ did not match at all. Interestingly the inverted film thickness for ‘chair down-up’ showed a profile with several sharp peaks over a cycle which was evidenced in the anodic transient although no clear alignment between peaks was noted. The observed current transients were also much larger for the daily living profiles than had been noted for the ISO walking profiles. This may have been a combination of the profiles’ severity and also the device had not been bedded-in with these profiles, meaning that the larger ranges of motion exposed

new areas of the bearing surface to articulation.

There is significant evidence emerging in the literature that simple gravimetric assessment of devices following cyclic continuous 1 Hz simulator testing is not necessarily a reliable indicator for real world *in-vivo* performance. For the industry gold standard MoP bearings the main failure mechanisms are reasonably well understood; i.e. wear debris induced osteolysis and aseptic loosening [26, 27]. As such a gravimetric wear rate and debris particle size distributions from simulator benchmarking may be useful for this bearing combination. For other materials, devices or bearing combinations with less understood or unknown failure mechanisms a much more thorough and systematic approach to testing is needed. Particularly for sliding interfaces with a metallic surface *in-situ* techniques such as electrochemistry are critical [18]. Comparing such devices’ gravimetric wear rates to a MoP design, as was done during pre-clinical testing of second-generation MoM [9, 10, 11, 12], is not useful.

de Villiers *et al.* [28] examined MoM bearings with *AgCrN* coatings in an orbital hip simulator and found *Co* and *Ag* ions present in the lubricant after testing despite negligible gravimetric material loss. Saikko *et al.* [29, 30] examined various adverse loading techniques across different devices and bearing combinations. Unless the test condition exceeded a devices’ ‘endurance limit’ gravimetrically determined wear rates generally displayed low variance between tests. The present authors have also examined the effects of adverse loading scenarios such as microseparation and found an order of magnitude increase in electrochemical degradation compared to two to four fold increases in gravimetric wear reported in the literature [17]. This suggests a shift in the importance of corrosion to total material loss and

may be a more important indicator of the performance of MoM prostheses which fail due to metallosis, ALVAL, ARMD and pseudotumors [31, 32, 33, 34, 35].

435 Simulator design is also improving with next generation 470 simulators capable of more axes of motion and wider operating profiles. This will enable future testing to incorporate adverse loading and daily living cycles to great effect. When comparing these new simulators to the previous generation however, a more 440 complicated three-axes of motion Full-ISO walking profile only marginally increased the reported gravimetric wear [36] and was used to justify the continued use of the previous generation. With the new simulators a new 445 generation of pre-clinical assessment is needed. *In-situ* methods for assessing material loss and more varied testing regimes than continuous 1 Hz articulation. 480

Coupled with improved testing techniques there also needs to be a greater understanding on how tribological systems can affect total material loss. The 450 modelling of interfaces with metallic surfaces has therefore been a focus in the literature. Cao *et al.* [37, 38] recently presented a new model which attempted to combine and predict mechanical and chemical mass loss for 455 MoM bearings. The model shows a good correlation with gravimetric wear rates reported in the literature for MoM simulator studies [38]. The model only achieved 490 this by considering the steady-state wear which, as discussed, is not necessarily a good indicator of MoM performance. 460

The Cao model predicts the degradation of MoM bearings to be electrochemically dominant which has 495 not been found to be the case for 28 or 36 mm bearings in simulators instrumented with a three-electrode electrochemical cell [16, 17, 19, 20]. Looking closely 465 at the degradation over a cycle the Cao model also

shows points of zero electrochemical degradation which roughly align with the maximum anodic current peaks observed in the present study [37]. Another new model proposed by Gao *et al.* [39, 40] also incorporated 475 tribo-corrosion as a pathway to material loss and successfully predicted a typical running-in and steady-state wear pattern. The Gao model suggests the wear rate is highly dependant on EHL film thickness which can change as a result of material loss.

Whilst there has been much success, a tribocorrosive contact is an incredibly complicated interface and difficult to model and predict. As evidenced by the simplified 2D model used in this study. There was some success correlating the model with an ISO walking profile, but it was not capable of describing the more 480 complicated daily living cycles. Existing models in the literature are improving but don't always agree with experimental data. More work is therefore needed as a comprehensive 3D tribocorrosion model, validated with 485 *in-situ* experimental techniques, would be an incredibly powerful tool for pre-clinical assessment of devices and assisting patient selection.

5. Conclusions

490 A simplified 2D Hamrock-Dowson model correlated well with measured anodic current transients from a Metal-on-Metal bearing articulated under bed-in and steady-state conditions, demonstrating a clear and important link between the tribology and corrosive degradation of these devices.

- The corrosive degradation of a MoM bearing under sliding is closely linked to the tribological conditions at a given point in a cycle.

- Peaks in current, and thus depassivation, occur at the same point in the cycle despite cycle frequency.
- The Theoretical Minimum Film Thickness calculated using a simplified 2D model appeared very similar in both shape and magnitude to anodic current transients.
- A more detailed comprehensive 3D model is required to fully describe the tribology and depassivation under more complex daily living cycles.

References

- [1] Beadling, A.R.. A Link Between the Tribology and Corrosive Degradation of Metal-on-Metal THRs - Supporting Data. University of Leeds [Dataset]; 2016. doi:<http://doi.org/10.5518/88>.
- [2] National Joint Registry, . NJR 9th Annual Report for England, Wales and Northern Ireland. 2012.
- [3] National Joint Registry, . NJR 10th Annual Report for England, Wales and Northern Ireland. 2013.
- [4] National Joint Registry, . NJR 12th Annual Report: Prostheses used in hip, knee, ankle, elbow and shoulder replacement procedures 2014. 2015.
- [5] Bowsher, J.G., Hussain, A., Williams, P.A., Shelton, J.C.. Metal-on-metal hip simulator study of increased wear particle surface area due to 'severe' patient activity. *Proc Inst Mech Eng H* 2006;220(2):279–87.
- [6] Angadji, A., Royle, M., Collins, S.N., Shelton, J.C.. Influence of cup orientation on the wear performance of metal-on-metal hip replacements. *Proc Inst Mech Eng H* 2009;223(4):449–57.
- [7] Williams, S., Leslie, I., Isaac, G., Jin, Z., Ingham, E., Fisher, J.. Tribology and wear of metal-on-metal hip prostheses: influence of cup angle and head position. *JBJSAm* 2008;90 Suppl 3:111–7.
- [8] Al-Hajjar, M., Williams, S., Fisher, J., Jennings, L.M., Lim, C.T., Goh, J.C.H.. The Influence of Cup Inclination Angle and Head Position on the Wear of Metalon-Metal Bearings in Total Hip Replacements. In: 6th World Congress of Biomechanics. Singapore; 2010, p. 752–5.
- [9] Anissian, H.L., Stark, A., Gustafson, A., Good, V., Clarke, I.C.. Metal-on-metal bearing in hip prosthesis generates 100-fold less wear debris than metal-on-polyethylene. *Acta Orthop Scand* 1999;70(6):578–82.
- [10] Goldsmith, A.A.J., Dowson, D., Isaac, G.H., Lancaster, J.G.. A comparative joint simulator study of the wear of metal-on-metal and alternative material combinations in hip replacements. *Proc Inst Mech Eng H* 2000;214(1):39–47.
- [11] Jin, Z.M., Firkins, P., Farrar, R., Fisher, J.. Analysis and modelling of wear of cobalt-chrome alloys in a pin-on-plate test for a metal-on-metal total hip replacement. *Proc Inst Mech Eng H* 2000;214(6):559–68.
- [12] Scholes, S.C., Green, S.M., Unsworth, A.. The wear of metal-on-metal total hip prostheses measured in a hip simulator. *Proc Inst Mech Eng H* 2001;215(6):523–530.
- [13] Smith, A.J., Dieppe, P., Howard, P.W., Blom, A.W., National Joint Registry, . Failure rates of metal-on-metal hip resurfacings: analysis of data from the National Joint Registry for England and Wales. *Lancet* 2012;380(9855):1759–66.
- [14] Yan, Y., Neville, A., Dowson, D., Williams, S., Fisher, J.. Effect of metallic nanoparticles on the biotribocorrosion behaviour of Metal-on-Metal hip prostheses. *Wear* 2009;267(5-8):683–8.
- [15] Yan, Y., Neville, A., Dowson, D., Williams, S., Fisher, J.. The influence of swing phase load on the electrochemical response, friction, and ion release of metal-on-metal hip prostheses in a friction simulator. *Proc Inst Mech Eng J* 2009;223(3):303–9.
- [16] Hesketh, J., Hu, X., Yan, Y., Dowson, D., Neville, A.. Biotribocorrosion: Some electrochemical observations from an instrumented hip joint simulator. *Tribology International* 2013;59:332–8.
- [17] Beadling, A., Bryant, M., Dowson, D., Neville, A.. The Effect of Microseparation on Corrosion Rates of Metal-on-Metal Total Hip Replacements. In: *Corrosion*. Dallas, TX: NACE International; 2015, p. 12.
- [18] Neville, A., Hesketh, J., Beadling, A.R., Bryant, M.G., Dowson, D.. Incorporating corrosion measurement in hip wear simulators: An added complication or a necessity? *Proc Inst Mech Eng H* 2016;230(5):406–20.
- [19] Hesketh, J.. Tribocorrosion of Total Hip Replacements. Ph.D. thesis; University of Leeds; 2012.
- [20] Hesketh, J., Meng, Q., Dowson, D., Neville, A.. Biotribocorrosion of metal-on-metal hip replacements: How surface degradation can influence metal ion formation. *Tribology Inter-*

- national 2013;65:128–37.
- 580 [21] International Standards Organisation, . ISO 14242-1:2014 - Implants for surgery - Wear of total hip-joint prostheses - Part 1: Loading and displacement parameters for wear-testing machines and corresponding environmental conditions for test. 2014. 625
- [22] Fabry, C., Herrmann, S., Kaehler, M., Klinkenberg, E.D., Woernle, C., Bader, R.. Generation of physiological parameter sets for hip joint motions and loads during daily life activities for application in wear simulators of the artificial hip joint. Med 585 Eng Phys 2013;35(1):131–9. 630
- [23] Bergmann, G., Deuretzbacher, G., Heller, M., Graichen, F., Rohlmann, A., Strauss, J., et al. Hip contact forces and gait patterns from routine activities. J Biomech 2001;34:859–71. 590
- [24] Bergmann, G., Graichen, F., Rohlmann, A., Bender, A., Heinlein, B., Duda, G.N., et al. Realistic loads for testing hip implants. Biomed Mater Eng 2010;20(2):65–75. 635
- 595 [25] Hamrock, B.J., Dowson, D.. Elastohydrodynamic lubrication of elliptical contacts for materials of low elastic modulus: 1 fully flooded conjunction. Trans ASME, J Lubric Tech 1978;100:236–45. 640
- [26] Ingham, E., Fisher, J.. Biological reactions to wear debris in total joint replacement. Proc Inst Mech Eng H 2000;214:21–37. 600
- [27] Ingham, E., Fisher, J.. The role of macrophages in osteolysis of total joint replacement. Biomaterials 2005;26:1271–86. 645
- [28] de Villiers, D., Shelton, J.C.. Measurement outcomes from hip simulators. Proc Inst IMechE H 2016;230:398–405.
- 605 [29] Saikko, V., Ahlroos, T., Revitzer, H., Ryti, O., Kuosmanen, P.. The effect of acetabular cup position on wear of a large-diameter metal-on-metal prosthesis studied with a hip joint simulator. Tribology International 2013;60:70–6. 650
- [30] Saikko, V.. Effect of increased load on the wear of a large diameter metal-on-metal modular hip prosthesis with a high inclination angle of the acetabular cup. Tribology International 2016;96:149–154.
- [31] Park, Y.S., Moon, Y.W., Lim, S.J., Yang, J.M., Ahn, G., Choi, Y.L.. Early osteolysis following second-generation metal-on-metal replacement. JBJSAm 2005;87:1515–21. 615
- [32] Willert, H.G., Buchhorn, G.H., Fayyazi, A., Flury, R., Windler, M., Kster, G., et al. Metal-on-metal bearings and hypersensitivity in patients with artificial hip joints. A clinical and histomorphological study. JBJSAm 2005;87:28–36.
- 620 [33] Korovessis, P., Petsinis, G., Repanti, M., Repantis, T.. Metallosis after contemporary metal-on-metal total hip arthroplasty. Five to nine-year follow-up. JBJSAm 2006;88:1183–91.
- [34] Watters, T.S., Cardona, D.M., Menon, K.S., Vinson, E.N., Bolognesi, M.P., Dodd, L.G.. Aseptic lymphocyte-dominated vasculitis-associated lesion: a clinicopathologic review of an underrecognized cause of prosthetic failure. Am J Clin Pathol 2010;134:886–93.
- [35] Campbell, P.A., Ebramzadeh, E., Nelson, S., Takamura, K., De Smet, K.A., Amstutz, H.C.. Histological Features of Pseudotumor-like Tissues From Metal-on-Metal Hips. Clin Orthop Relat Res 2010;468:2321–27.
- [36] Ali, M., Al-Hajjar, M., Partridge, S., Williams, S., Fisher, J., Jennings, L.M.. Influence of hip joint simulator design and mechanics on the wear and creep of metal-on-polyethylene bearings. Proc Inst IMechE H 2016;230(5):389–97.
- [37] Cao, S., Guadalupe Maldonado, S., Mischler, S.. Tribocorrosion of passive metals in the mixed lubrication regime: theoretical model and application to metal-on-metal artificial hip joints. Wear 2015;324325:55–63.
- [38] Cao, S., Mischler, S.. Assessment of a recent tribocorrosion model for wear of metal-on-metal hip joints: Comparison between model predictions and simulator results. Wear 2016;362-363:170–8.
- [39] Gao, L., Dowson, D., Hewson, R.W.. Predictive Wear Modelling of the Articulating Metal-on-Metal Hip Replacements. J Biomed Mater Res B 2015;In press:1–10. doi:10.1002/jbm.b.33568.
- [40] Gao, L., Dowson, D., Hewson, R.W.. A numerical study of non-Newtonian transient elastohydrodynamic lubrication of metal-on-metal hip prostheses. Tribology International 2016;93(Part B):486–94.